Inverse magnetocaloric effect in Heusler Ni44.4Mn36.2Sn14.9Cu4.5 alloy at low temperatures

Alexander P. Kamantsev *, Yuriy S. Koshkid'ko, Ruslan Yu. Gaifullin, Irek I. Musabirov, Anatoliy V. Koshelev, Alexey Victorovich Mashirov, Vladimir V. Sokolovskiy, Vasiliy D. Buchelnikov, Jacek Ćwik, Vladimir G. Shavrov

Posted Date: 13 October 2023

doi: 10.20944/preprints202310.0715.v1

Keywords: metamagnetic phase transition; magnetocaloric effect; Heusler alloys; Monte Carlo calculations.

Article

Inverse Magnetocaloric Effect in Heusler $Ni_{44.4}Mn_{36.2}Sn_{14.9}Cu_{4.5}$ Alloy at Low Temperatures

Alexander P. Kamantsev [1,*], Yuriy S. Koshkid'ko [2], Ruslan Yu. Gaifullin [3], Irek I. Musabirov [3], Anatoliy V. Koshelev [4], Alexey V. Mashirov [1], Vladimir V. Sokolovskiy [5,6], Vasiliy D. Buchelnikov [5], Jacek Ćwik [2] and Vladimir G. Shavrov [1]

[1] Kotelnikov Institute of Radioengineering and Electronics of Russian Academy of Sciences, 125009 Moscow, Russia; a.v.mashirov@mail.ru (A.V.M.); shavrov@cplire.ru (V.G.S.)
[2] Institute of Low Temperature and Structure Research of Polish Academy of Sciences, 50-422 Wroclaw, Poland; y.koshkidko@intibs.pl (Y.S.K.); j.cwik@intibs.pl (J.C.)
[3] Institute for Metals Superplasticity Problems of Russian Academy of Sciences, 450001 Ufa, Russia; gaifullin_1998@bk.ru (R.Y.G.); irekmusabirov@mail.ru (I.I.M.)
[4] Institute of Experimental Mineralogy of Russian Academy of Sciences, 142432 Chernogolovka, Russia; anatolkosh@mail.ru
[5] Department of Condensed Matter Physics, Chelyabinsk State University, 454001 Chelyabinsk, Russia; vsokolovsky84@mail.ru (V.V.S.); buche@csu.ru (V.D.B.)
[6] Academic Research Center for Energy Efficiency, National University of Science and Technology "MISIS", 119049 Moscow, Russia
* Correspondence: kaman4@gmail.com

Abstract: The direct measurements of the magnetocaloric effect were performed in Heusler $Ni_{44.4}Mn_{36.2}Sn_{14.9}Cu_{4.5}$ alloy at cryogenic temperatures in magnetic fields up to 10 T. The maximum value of the inverse magnetocaloric effect in a field of 10 T was observed ΔT_{ad} = –2.7 K in the vicinity of the 1st order magnetostructural phase transition at T_0 = 117 K. The *ab initio* and Monte Carlo calculations were performed to discuss the effect Cu doping into Ni-Mn-Sn compound on the ground state structural and magnetic properties. It is shown that with increasing Cu content the martensitic transition temperature decreases and the Curie temperature of austenite slightly increases. In general, calculated transition temperatures, magnetization values are correlated well with the experimental ones.

Keywords: metamagnetic phase transition; magnetocaloric effect; Heusler alloys; Monte Carlo calculations

1. Introduction

The promising idea of solid-state magnetic cooling (SMC) by means of adiabatic demagnetization of paramagnetic salts was used in the early 1930s to develop new methods to obtain the low temperatures below 1 K [1]. The SMC is based on the magnetocaloric effect (MCE), which is a reversible change in an entropy ΔS_{iso} under isothermal conditions or in a temperature ΔT_{ad} under adiabatic conditions of a magnetic material due to the external magnetic field changes [2,3]. The MCE is an efficient tool in the study of magnetic phase transitions (PTs), which is among the most urgent problems in modern solid-state physics. The maximum of the MCE is reached in the vicinity of magnetic PTs [3,4]. The magnetic materials with magnetic PTs in the required range of working temperatures are chosen for SMC. The promising applications of the SMC at low temperatures in particular for the liquefaction of gases such as N_2, He, H_2 or natural gases have been mentioned in [5,6]. The advantages of such materials for SMC at low temperatures are related to the fact that the magnetic heat capacity increases in the region of the magnetic PT and becomes comparable (and sometimes exceeds) to the heat capacity of the crystal lattice of a solid. This circumstance makes SMC more promising at low temperatures, where the lattice heat capacity of metals is much higher than that at room temperature. It is commonly accepted at present that low (cryogenic) temperatures are temperatures below 120 K [7].

 doi:10.20944/preprints202310.0715.v1

The MCE can be either direct or inverse under a magnetization of a magnetic material [2–4]. The direct MCE is a decrease in entropy at isothermal conditions or an increase in temperature at adiabatic conditions. Against, the inverse MCE is a positive isothermal change in entropy or a negative adiabatic change in temperature under magnetization. Both direct and inverse MCE can be used for SMC at low temperatures. The inverse MCE can be useful when it is necessary to rapidly cool an area in the presence of magnetic field., It is sufficed to exert magnetic field on the refrigerant for this purpose. Thus, the refrigerant will cool down, and it will also cool the area of magnetic field. The effect can be used to cool a superconducting magnet and the surrounding liquefied gas [8], which will make it possible to reduce the consumption of liquefied gas.

The rare-earth metals [4] and their intermetallic compounds [9] are the most promising materials for SMC at low temperatures. The magnetostructural PTs in such alloys are normally observed at temperatures above 120 K [2]. Most often they show a direct MCE in the vicinity of the PTs. The inverse MCE is observed in their intermetallic compounds with antiferromagnetic (AFM) ordering: RCu_2, R_2Fe_{17}, RFe_3 (R – heavy rare-earth metal) [9,10], Gd_2In [11]. The inverse MCE can also be observed as a result of magnetization rotation upon magnetization of a highly anisotropic single-crystal sample along the hard magnetization axis in RCo_5 and Tb–Gd [12,13]. However, the rare earth metals are expensive, and their compounds are breakable and rapidly oxidize on the air, so they are difficult to use in the proposed scheme of the SMC.

Inverse MCE at low temperatures can also be exhibited by Mn-based compounds, for example in Mn_5Si_3 [14]. Significant inverse MCE can be observed in several ferromagnetic (FM) Heusler alloys based on Ni–Mn–Z (Z = In, Sb, Sn), but usually they show it closer to the room temperatures [15–18]. Some compositions of the Heusler alloys show the inverse MCE at low temperatures, for example the Ni(-Co)-Mn-Ti Heusler alloys [19]. We investigated the $Ni_{44.4}Mn_{36.2}Sn_{14.9}Cu_{4.5}$ Heusler alloy with the inverse MCE at low temperature perspective for the SMC and tried to explain its properties theoretically in this paper.

2. Materials and Methods

2.1. Samples Characterization

Initially, the composition of the Heusler alloy was chosen according to [20]. Polycrystalline ingot of the $Ni_{44.4}Mn_{36.2}Sn_{14.9}Cu_{4.5}$ Heusler alloy was synthesized by the argon arc-melting method from high purity elements. The ingot was remelted seven times for the elimination the chemical segregation of the composition. The obtained ingot had the mass of about 80 g. The samples in the form of the 1 mm thick plates were cut and sealed into evacuated quartz ampoules. As is shown earlier the melting point this alloy is 1313 K [21] due to the temperature of the homogenization annealing was selected as 1133 K. The sealed samples were subjected to homogenization annealing for 24 hours, after that they were quenched in water.

The X-ray diffraction and the X-ray phase analysis was performed on a Rigaku Ultima V X-ray diffractometer using Cu-Kα radiation. The crystal structure of the studied sample at room temperature is cubic (space group *Fm-3m*) with lattice parameter a_0 = 5.991 A.The analysis of the microstructure and elemental composition were carried out on a Vega 3-SBH Tescan scanning electron microscope (SEM) equipped with sensors for the backscattered electrons and the energy-dispersive X-ray (EDX) analysis (Oxford Instruments). The specimens were prepared by electropolishing in an electrolyte with 90 % n-butyl alcohol (C_4H_9OH) and 10 % HCl. The microstructure of the alloy by SEM is represented by a single-phase state and is shown in Figure 1a. The dark points on the thin section are etching pits. The grains have size in order of 100 μm according to the orientational contrast. The microstructure can be characterized as an equiaxed one in general. The not blurred contrast means that the grain boundaries are high-angle ones. The chemical elements maps of the section area are obtained by EDX analysis and presented in Figure 1b. The distribution of the Ni, Mn, Sn and Cu is uniform, and the areas with localization of the any elements are absent. It can be concluded, that annealing at 1133 K for 24 hours followed by quenching makes possibly to obtain a single-phase state of the sample so within the possibility of EDX analysis.

Preprints (www.preprints.org) | NOT PEER-REVIEWED | Posted: 13 October 2023 doi:10.20944/preprints202310.0715.v1

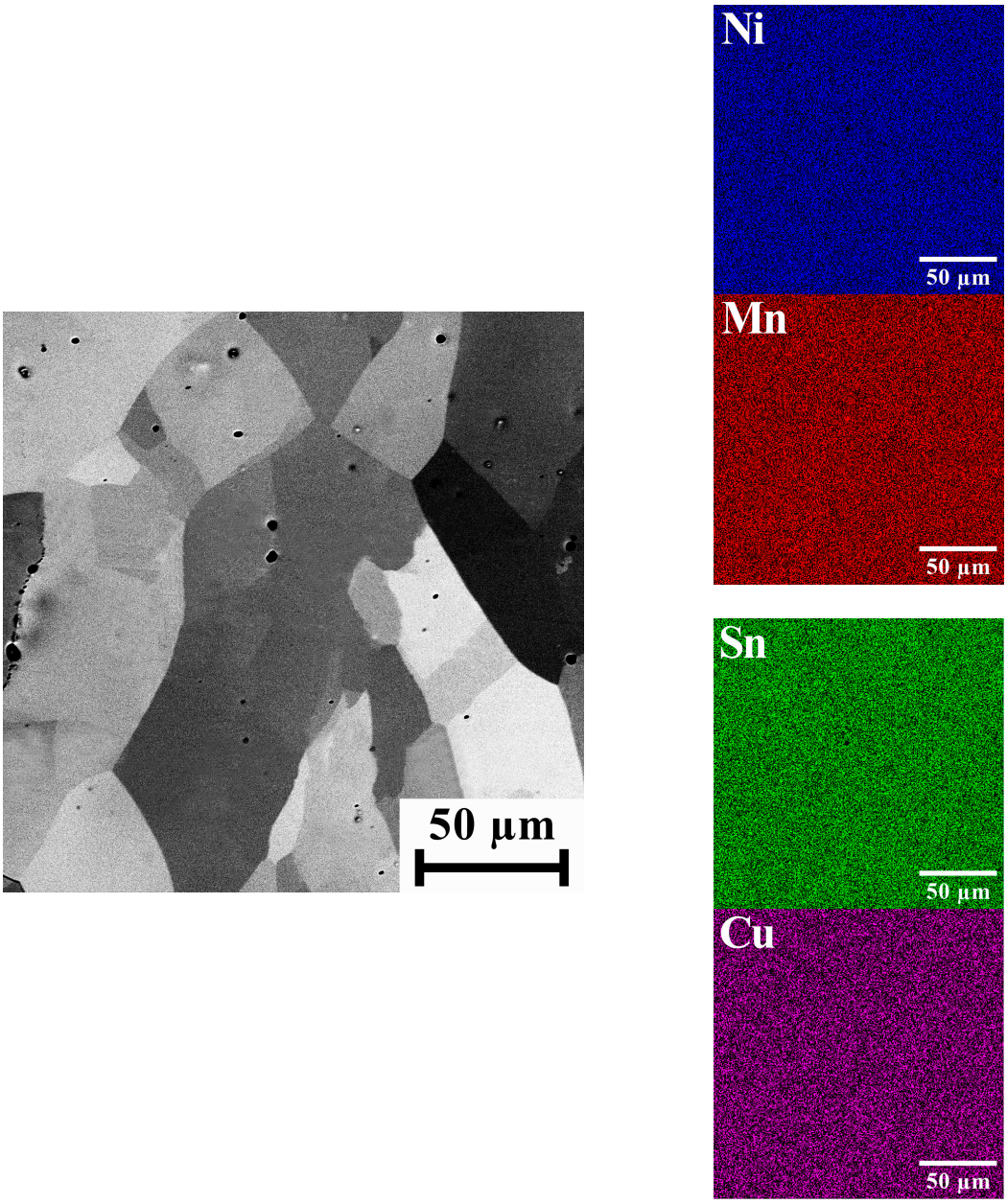

Figure 1. (a) Microstructure of the $Ni_{44.4}Mn_{36.2}Sn_{14.9}Cu_{4.5}$ Heusler alloy is obtained by SEM. **(b)** Maps of the chemical element's distribution of the section area of the $Ni_{44.4}Mn_{36.2}Sn_{14.9}Cu_{4.5}$ Heusler alloy are obtained by EDX analysis.

The magnetic properties of $Ni_{44.4}Mn_{36.2}Sn_{14.9}Cu_{4.5}$ Heusler alloy samples were studied by standard magnetometry methods (ZFC-FC-FH protocols) using a SQUID magnetometer in low magnetic field of 10 mT (inset in Fig.1a) and in fields of 1 T and 3 T in wide temperature range of 2–400 K (Figure 1a). The alloy demonstrates two magnetic PTs of the 1st and the 2nd orders. The magnetostructural PT of the 1st order from a ferrimagnetic (FiM) martensitic phase to a FM austenitic phase is observed at the cryogenic temperatures. The characteristic start and finish temperatures of the martensite and the austenite states obtained by the tangential method and are denoted as M_S = 101 K, M_F = 54 K, A_S = 70 K, and A_F = 118 K, respectively. The temperature hysteresis about 20 K is observed during the heating/cooling process (inset in Fig.1a). The application of high magnetic fields shifts the region of the martensitic phase to lower temperatures with the rate of –2.2 K/T (Figure 1a), which makes it possible to realize the inverse MCE in this alloy in relatively low magnetic fields at cryogenic temperatures. The magnetic PT of the 2nd order is the Curie temperature at $T_C \approx 350$ K.

Preprints (www.preprints.org) | NOT PEER-REVIEWED | Posted: 13 October 2023 doi:10.20944/preprints202310.0715.v1

Magnetic field dependence of the magnetization of the $Ni_{45.3}Mn_{35.9}Sn_{14.3}Cu_{4.5}$ Heusler alloy for different temperatures in the vicinity of the magnetostructural PT from 50 to 130 K with increasing and decreasing of the magnetic fields are shown in Figure 2b. The results were obtained in Bitter magnet's magnetic fields up to 10 T by using an original technique detail described in [22].

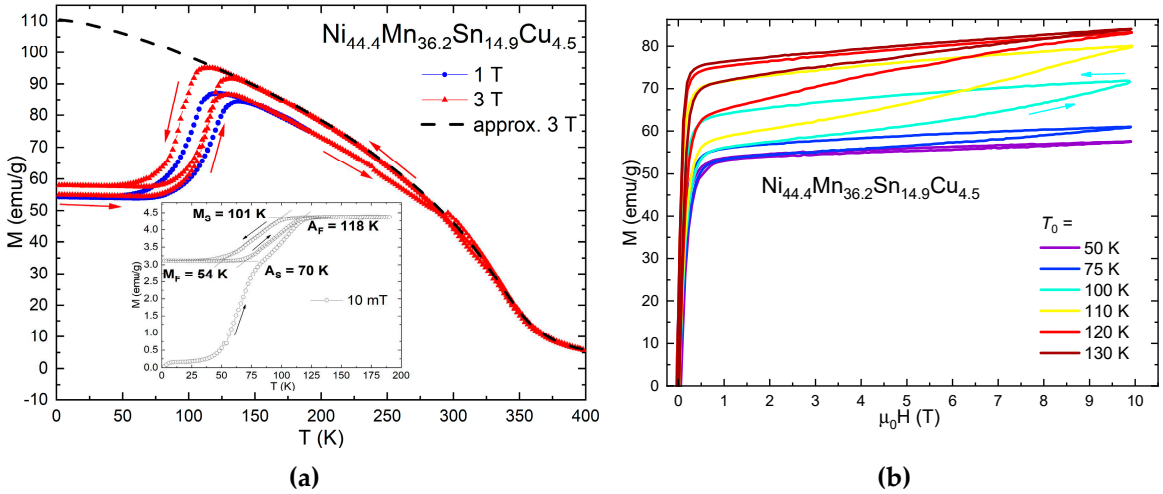

(a) **(b)**

Figure 2. (a) Temperature dependences of the magnetization of the $Ni_{45.3}Mn_{35.9}Sn_{14.3}Cu_{4.5}$ Heusler alloy in high magnetic fields of 1 and 3 T, inset: in low field of 10 mT. The dashed line are calculated curve (approximation) of the temperature dependence of the magnetization in $\mu_0 H$ = 3 T for the sample in austenite phase (without a magnetostructural PT). **(b)** Field dependences of the magnetization of the $Ni_{45.3}Mn_{35.9}Sn_{14.3}Cu_{4.5}$ Heusler alloy at different temperatures from 50 to 130 K are obtained with increasing and decreasing of the field.

2.2. Computational Methods

In order to study the role of Cu addition on the structural and magnetic properties of Ni-Mn-Sn alloy, we also carried out theoretical studies in the framework of ab initio calculations and Monte Carlo (MC) simulations.

First-principles calculations of the ground state properties of the austenitic and martensitic phases of Cu-doped Ni-Mn-Sn alloys were performed using the projector augmented wave (PAW) method implemented in the VASP package [23,24]. The generalized gradient approximation in the formulation of Perdue, Burke, and Ernzerhof [25] was chosen to calculate the exchange-correlation energy. Electron-ion interactions are described by PAW potentials with the electronic configurations as follows: $3p^6 3d^8 4s^2$ for Ni, $3p^6 3d^6 4s^1$ for Mn, $3d^{10} 4s^2 4p^2$ for Sn, and $3p^6 3d^{10} 4s^1$ for Cu. The cutoff energy of plane waves was 450 eV. The Brillouin zone was sampled by a 5×5×4 mesh of k points centered at Gamma point. The convergence criteria for the total energy is 10^{-6} eV/at. A 2×2×2 supercell of 64 atoms with 8 atom tetragonal unit cell ($L1_0$, $Im\bar{3}m$, #139) was considered.

The geometric optimization procedure was carried out for the compounds $Ni_{32-x}Cu_xMn_{23}Sn_9$ (x = 1, 2, and 3), which correspond to $Ni_{50-x}Cu_xMn_{35.94}Sn_{14.06}$ (x = 1.56, 3.12 и 4.69 at.%), where the latter is close to the experimental $Ni_{44.4}Cu_{4.5}Mn_{36.2}Sn_{14.9}$. Two magnetic configurations were considered: FM, where the Mn_1, Mn_2 and Ni magnetic moments are parallelly aligned, and FiM, where magnetic moments of Mn_2 atoms are reversed with respect to the Mn_1 and Ni magnetic moments. Here Mn_1 and Mn_2 are Mn atoms located in the regular Mn sublattice and Sn sublattice, respectively.

The spin polarized relativistic Korringa-Kohn-Rostoker code implemented in the SPR-KKR package [26] was applied for calculating of the magnetic exchange coupling constants in austenitic and martensitic phase of Ni-Cu-Mn-Sn. The formation of non-stoichiometric compositions was performed in the coherent potential approximation. Brillouin zone integration was performed using a special point method on a 57×57×57 k-grid (4495 k-points) to calculate self-consistent potentials and exchange interaction integrals, respectively. The energy convergence threshold was set to 0.01 mRy.

Preprints (www.preprints.org) | NOT PEER-REVIEWED | Posted: 13 October 2023 doi:10.20944/preprints202310.0715.v1

The temperature dependencies of the magnetization were modeled using the MC method, the Heisenberg Hamiltonian and Metropolis algorithm [27]. The model lattice with periodic boundary conditions is consisted of 5488 atoms (for Ni_2MnSn: 2744 Ni atoms, 1372 Mn and Ga atoms) and is obtained by multiplying 7×7×7 times the 16-atom unit cell. To form $Ni_{50-x}Cu_xMn_{35.94}Sn_{14.06}$ (x = 1.56, 3.12 и 4.69 at.%), the Mn_2 and Cu atoms were randomly distributed at Sn and Ni sites. The number of MC steps per temperature value was 1×10^5. To achieve thermal equilibrium in the system, the first 10^4 steps of the MC were discarded. Magnetization averaging was performed for 225 configurations for every 400 MC steps.

3. Results

3.1. Indirect MCE Estimation

The isothermal change of magnetic entropy ΔS_{iso} was obtained from Maxwell's thermodynamic relations (1) by using the magnetization curves with increasing of field from 0 to 10 T and presented in Figure 2b.

$$\Delta S_{iso} = \int_0^H \left(\frac{\partial M(T,H)}{\partial T}\right)_H dH. \quad (1)$$

The maximum value of the magnetic entropy change was ΔS_{iso} = 9.5 J/(kg K) at T = 113 K in $\mu_0 H$ = 10 T (Figure 3a). The ΔS_{iso} values obtained in the vicinity of hysteresis of the magnetostructural PT are irreversible, because reversible MCE values in this region can be obtained by demagnetizing of the sample or by turning on the magnetic field again.

The isothermal heat ΔQ is also an important parameter of the working body of a magnetic refrigerator, it allows to estimate the amount of heat that can be taken from the cooled bath as a result of one ideal cycle of the isothermal magnetization/demagnetization processes. Figure 3b shows the ΔQ values calculated from the ΔS_{iso} values by using Equation (2)

$$\Delta Q = -T\Delta S_{iso}, \quad (2)$$

The maximum value was ΔQ = 1.06 kJ/kg at T = 113 K in magnetic field of 10 T, which is an order of magnitude lower than the maximum known value for the MnAs compound at room temperature in the same magnetic field [28].

The presence of field hysteresis (Figure 2a) in the vicinity of the magnetostructural PT in the sample's magnetization/demagnetization cycle leads to irreversible heat release δQ, which was calculated by using the Equation (3)

$$\partial Q = \mu_0 \oint H dM. \quad (3)$$

Figure 3b shows the δQ values calculated for different temperatures with the maximal value δQ = 0.09 kJ/kg at T = 110 K. This value is only 8.5% of the ΔQ maximal value, which is made by the Heusler $Ni_{44.4}Mn_{36.2}Sn_{14.9}Cu_{4.5}$ alloy is interesting for using as a magnetocaloric working body in the temperature range of natural gas liquefaction [8], despite the presence of field hysteresis of the magnetostructural PT.

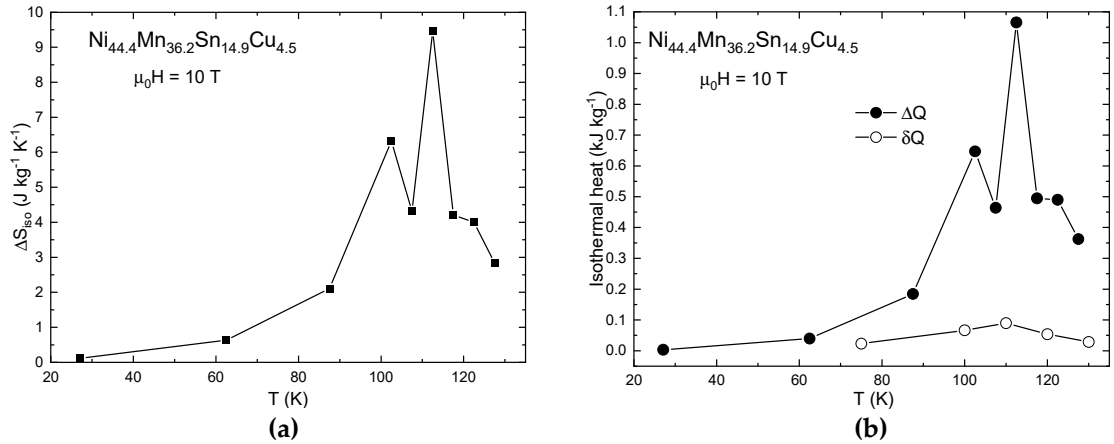

Preprints (www.preprints.org) | NOT PEER-REVIEWED | Posted: 13 October 2023 doi:10.20944/preprints202310.0715.v1

Figure 3. (a) Temperature dependence of the isothermal entropy changes ΔS_{iso} in the magnetic field $\mu_0 H$ = 10 T for the Heusler $Ni_{44.4}Mn_{36.2}Sn_{14.9}Cu_{4.5}$ alloy. **(b)** Temperature dependences of the isothermal heat ΔQ and the irreversible magnetization losses δQ in $\mu_0 H$ = 10 T for the Heusler $Ni_{44.4}Mn_{36.2}Sn_{14.9}Cu_{4.5}$ alloy.

3.2. Direct MCE Measurements

The extraction method in Bitter magnet's field up to 10 T was used for direct measurements of the MCE in the Heusler $Ni_{44.4}Mn_{36.2}Sn_{14.9}Cu_{4.5}$ alloy under adiabatic conditions ΔT_{ad}. This method in details was described in [29]. The studies were carried out in two different regimes: (1) sequential heating of the sample, (2) thermal cycling of the sample. In the first case, the sample temperature was successively raised and ΔT_{ad} was measured at selected temperatures. In the second case, the sample was pre-cooled down to 4.2 K, and then its temperature was raised to the required temperature for measurement. Figure 4 shows the results of measurements of the ΔT_{ad} value in magnetic fields of 1.8 T and 10 T: closed circles – sequential heating, open circles – thermal cycling.

The inverse MCE is observed in the region of low temperatures in a field of 1.8 T in both regimes of measuring (Figure 4). The maximum value of the inverse MCE in a field of 1.8 T was observed in the vicinity of the 1st order PT is ΔT_{ad} = –0.5 K at an initial temperature T_0 = 117 K (Figure 4). The inverse MCE increases with increasing of the magnetic field up to 10 T, reaching the value ΔT_{ad} = –2.7 K at T_0 = 117 K (Figure 4). It is interesting that direct MCE in a magnetic field of 10 T is observed in the FiM martensite phase and reaching the value ΔT_{ad} = 0.7 K (Figure 4) in the sequential heating regime in the temperature range of 20–60 K.

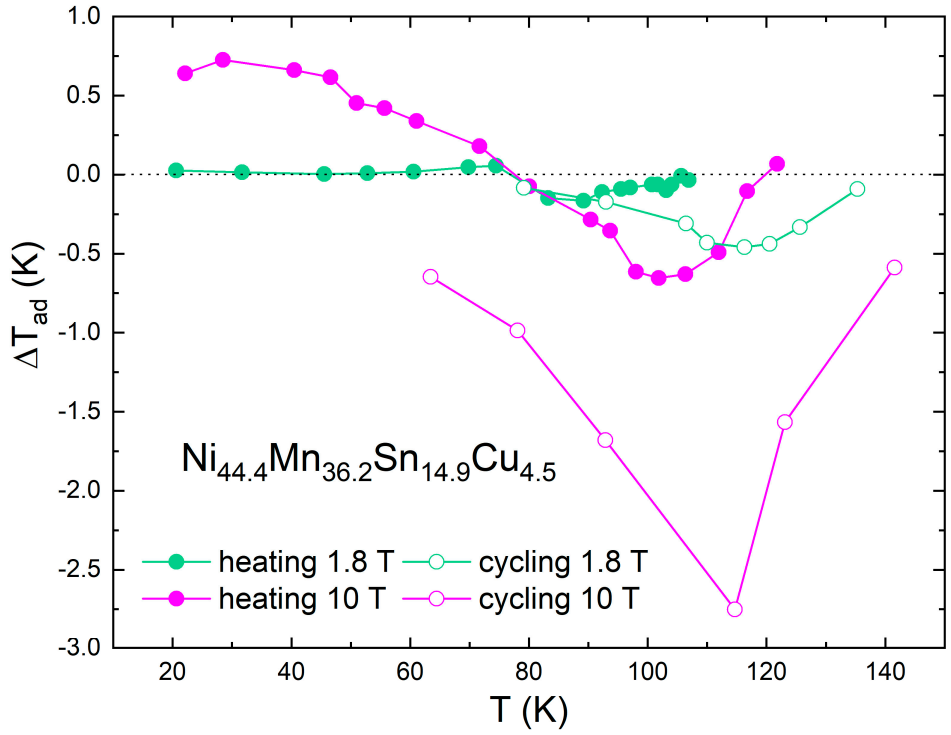

Figure 4. Temperature dependences of the adiabatic temperature change ΔT_{ad} for the $Ni_{44.4}Mn_{36.2}Sn_{14.9}Cu_{4.5}$ Heusler alloy, measured in magnetic fields of 1.8 T (green curves) and 10 T (violet curves) in two different regimes: the solid circles – during sequential heating of the sample, the open circles – after pre-cooling down to 4.2 K and subsequent heating to the measurement temperature.

Preprints (www.preprints.org) | NOT PEER-REVIEWED | Posted: 13 October 2023 doi:10.20944/preprints202310.0715.v1

3.3. Computational Results

We proceed to discuss the results of geometric optimization of the crystal structures of the austenitic and martensitic phases as well as the calculation of magnetic properties for Heusler $Ni_{50-x}Cu_xMn_{35.94}Sn_{14.06}$ alloys.

Figure 5 shows the energy landscape $E(c/a)$ of $Ni_{50-x}Cu_xMn_{35.94}Sn_{14.06}$ with response to volume-conserving elongations and compressions of the cubic $L2_1$ structure along c axis. The results are shown for both FM and FiM solutions (Figure 5a). One can see that the FM solution exhibits only one global cubic minimum at $c/a = 1$ being 11 meV/atom higher in energy than the FiM one and indicating an instability of FM tetragonal phase. For all compounds, the FiM ordering is energetically preferable compared to the FM one for both cubic austenitic and tetragonal martensitic phases. The global minimum for the FiM tetragonal phase takes place around $c/a = 1.25$.

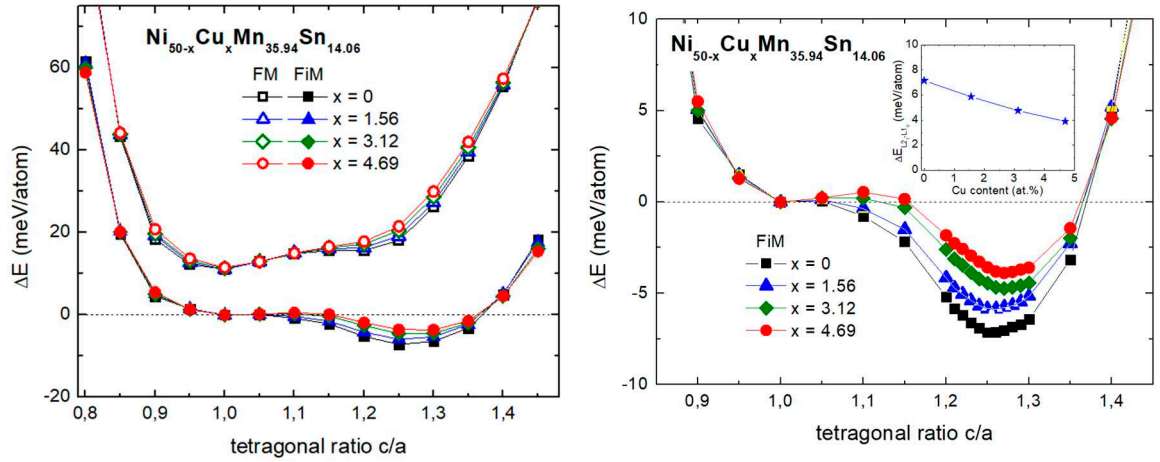

Figure 5. (a) Energy difference as function of the tetragonal c/a ratio for $Ni_{50-x}Cu_xMn_{35.94}Sn_{14.06}$ (x = 0, 1.56, 3.12, and 4.69). For all compounds, the energy zero corresponds to the FiM cubic structure. Filled and open symbols denote the FiM and FM solution, respectively. (b) Enlarged scale for the FiM solution. The Inset shows the energy difference between FiM cubic and tetragonal phases as a function of Cu content.

A close look at the FiM $E(c/a)$ curves, shown in Figure 5b, reveals that the c/a ratio of tetragonal phase varies slightly from 1.25 to 1.27 with increasing Cu content due to a reduce (an increase) of tetragonal lattice constant a_t (c), respectively (see Table 1). In addition, it is found that the optimized cubic lattice constant increases slightly with the addition of Cu. This is explained by the slightly larger atomic radius of Cu ($r = 1.28$ Å) compared to Ni ($r = 1.24$ Å). It should be noted that partial substitution of Ni by Cu reveals an almost linear decrease in the energy difference ($\Delta E_{L2_1-L1_0}$) between the FIM cubic and tetragonal structure, as evident from Figure 5b. For the parent compound with $x = 0$, $\Delta E_{L2_1-L1_0}$ is calculated to be 7.145 meV/atom, whereas in the case of x = 4.69 at.%, it reduces to 3.89 meV/atom. The decrease in the energy barrier with the Cu content indicates indirectly the reduce of the martensitic transition temperature T_m. The T_m temperature can be estimated from a rough approximation: $\Delta E_{L2_1-L1_0} \approx k_B T_m$ where k_B is the Boltzmann constant. According to this expression, $T_m \approx 83$ K for $Ni_{50}Mn_{35.94}Sn_{14.06}$ and 45 K for $Ni_{45.31}Cu_{4.69}Mn_{35.94}Sn_{14.06}$.

Table 1. Optimized lattice parameters and Debye temperatures of cubic and tetragonal structures of $Ni_{50-x}Cu_xMn_{35.94}Sn_{14.06}$. The Debye temperatures were calculated from elastic moduli.

Phase	Parameters	x=0	x=1.56	x=3.12	x=4.69
FiM cubic (c/a = 1)	a_0 (Å)	5.953	5.955	5.959	5.963
	Θ_D (K)	316	308	293	282
	a_t (Å)	5.526	5.513	5.502	5.500

Preprints (www.preprints.org) | NOT PEER-REVIEWED | Posted: 13 October 2023 doi:10.20944/preprints202310.0715.v1

FiM tetragonal (c/a = 1.27)	c (Å)	6.908	6.947	6.988	6.994
	c/a	1.25	1.26	1.27	1.27
	Θ_D (K)	333	325	308	295

A more correct way to estimate the martensitic transition temperature is to calculate the free energies of the austenitic and martensitic phases. For simplicity of calculations, we considered the lattice contribution to the free energy only, which at low temperatures plays a predominant role compared to the electronic and magnetic contributions:

$$F(T,V) = E(V) + F_{lat}(T,V), \quad (4)$$

where $E(V)$ is the ground state energy calculated at T = 0 K, $F_{lat}(T,V)$ is the lattice contribution calculated within the Debye model [30].

In Figure 6, we illustrate the free energies of $L2_1$ cubic and $L1_0$ tetragonal phases as well as the free energy difference $\Delta F = F_{L2_1} - F_{L1_0}$ for $Ni_{45.31}Cu_{4.69}Mn_{35.94}Sn_{14.06}$ alloy as an example. For $\Delta F > 0$, the $L1_0$ phase (matensite) is more preferable and *vica verse* for $\Delta F < 0$, the $L2_1$ phase (austenite) is stable. As evident from the figure, both free energy curves reveal a non-linear behavior with a temperature and intersect with each other at low temperature. The martensitic transition temperature extracted from ΔF = 0 is about 88 K, which agrees well with the experimental one (85.75 K) for $Ni_{44.4}Mn_{36.2}Sn_{14.9}Cu_{4.5}$, where T_m is computed via $T_m = (M_s + M_f + A_f + A_s)/4$. The low T_m temperature suggests that the zero-point vibrational energy ($\frac{9}{8}k_B\Theta_D$) plays a predominant role as compared to a vibrational entropy in the F_{lat} term. Thus, T_m is mainly contributed by $\Delta E_{L2_1-L1_0}$ at T = 0 K and $\Delta\Theta_D^{L2_1-L1_0}$ at $T > 0$ K. For $Ni_{45.31}Cu_{4.69}Mn_{35.94}Sn_{14.06}$, $\Delta\Theta_D^{L2_1-L1_0}$ is 13 K in absolute value. We would like to note that T_m is sensitive to $\Delta\Theta_D^{L2_1-L1_0}$, and an increase in $\Delta\Theta_D^{L2_1-L1_0}$ ($\Theta_D^{L2_1} < \Theta_D^{L1_0}$) leads to a reduce in T_m, the austenitic phase becomes stable in the whole temperature range at $\Delta\Theta_D^{L2_1-L1_0}$ is about 30 K in absolute value. On the hand, an increase in $\Delta\Theta_D^{L2_1-L1_0}$ ($\Theta_D^{L2_1} > \Theta_D^{L1_0}$) shifts T_m to higher temperatures.

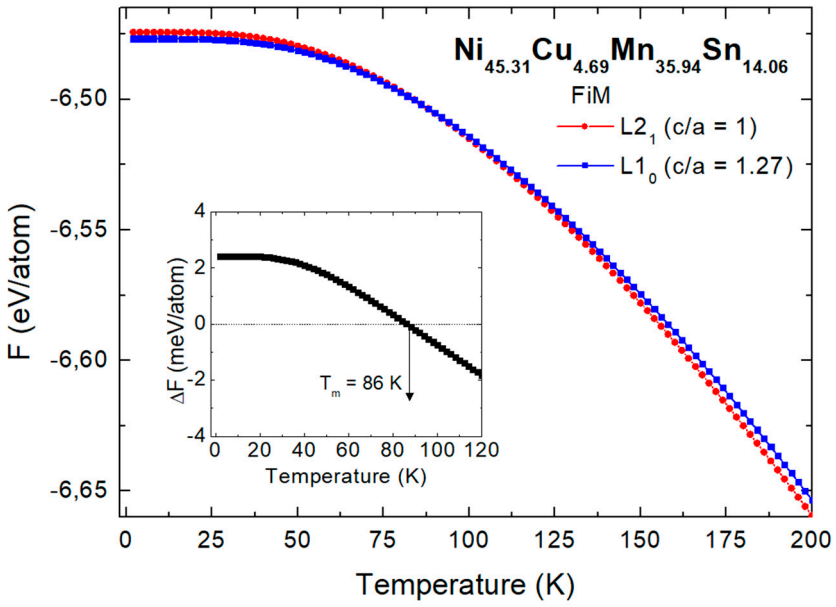

Figure 6. Temperature dependencies of the free energy of cubic and tetragonal phases of $Ni_{45.31}Cu_{4.69}Mn_{35.94}Sn_{14.06}$. The inset shows the free energy difference between $L2_1$ and $L1_0$ structures.

Figure 7 shows the pairwise exchange coupling constants J_{ij} as function of distance between i and j atoms for FiM-$L2_1$ and FiM-$L1_0$ $Ni_{45.31}Cu_{4.69}Mn_{35.94}Sn_{14.06}$ alloy as an example. We would like to note that magnetic interactions reveal a similar behavior for all compounds under study since Cu atoms are nonmagnetic. For both phases, intra-sublattice J_{ij} constants between Mn atoms (Mn_1-Mn_1 and Mn_2-Mn_2) show similar damped oscillatory behavior as a function of the distance between atoms

Preprints (www.preprints.org) | NOT PEER-REVIEWED | Posted: 13 October 2023 doi:10.20944/preprints202310.0715.v1

up to $d/a \approx 2$, except that J_{ij} (Mn_2-Mn_2) within the 1st and the 2nd coordination shell of the cubic structure exhibits the AFM character.

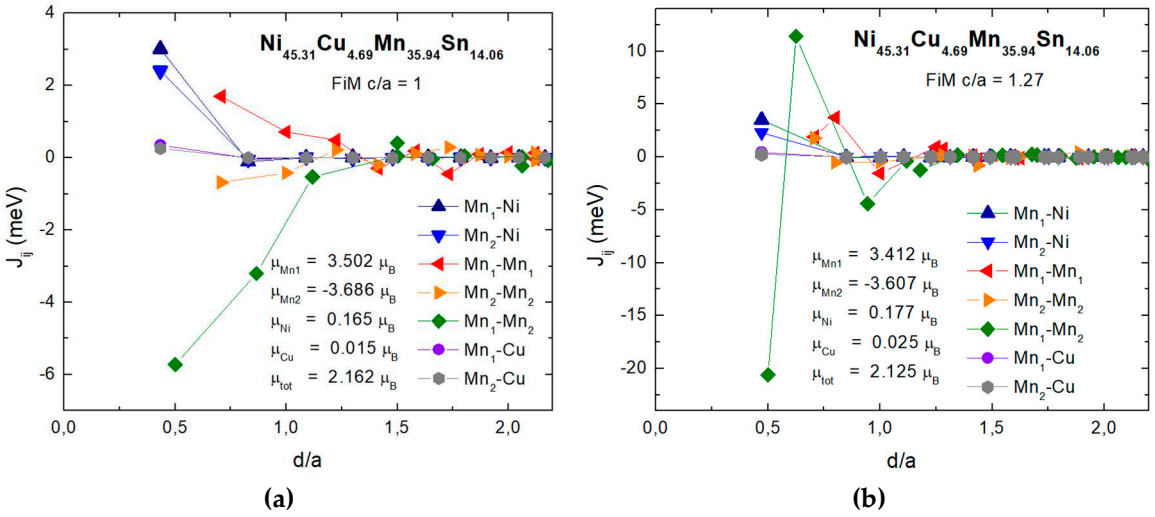

Figure 7. Calculated magnetic exchange parameters of (a) FiM $L2_1$- and (b) $L1_0$-$Ni_{45.31}Cu_{4.69}Mn_{35.94}Sn_{14.06}$ as functions of the distance between the atoms in units of the lattice constant a. Positive J_{ij} denote FM interactions, negative ones denote AFM interactions.

The cubic inter-sublattice interactions between the nearest Mn_1-Mn_2 atoms located at a smaller distance (d/a = 0.5) compared to the nearest pairs $Mn_{1(2)}$-$Mn_{1(2)}$ ($d/a = \sqrt{2}/2$) are characterized by a strong AFM interaction, which gradually decreases with increasing d/a. In contrast to cubic structure, the strongest AFM exchange (≈ - 20 meV) between the four nearest atoms Mn_1-Mn_2 located in the (110) plane is found for tetragonal structure due to the smallest distance (d/a = 0.5), whereas two next nearest atoms Mn_1-Mn_2 ($d/a \approx 0.627$) strongly interact ferromagnetically with $J_{ij} \approx 11.5$ meV. As for the $Mn_{1(2)}$-Ni interactions, they show similar behavior for both phases, demonstrating the FM exchange only between the nearest neighbors. Generally, the behavior of J_{ij} coupling constants is a similar to those of Ni-Mn-(Ga, In, Sb) alloys reported previously [31–34].

Let us make a general remark concerning the behavior of the exchange interaction parameters for the remaining compounds in the cubic and tetragonal phases. Since the substitution of Ni by Cu influences a small change in the parameters of crystal structures for both phases, it will also affect weakly the exchange constants between the nearest pairs of Ni Mn_1, Mn_2 (See Table 2). For cubic structure, a slight enhancement of the FM interactions $J_{Mn1(2)\text{-}Mn1(2)}$ and $J_{Mn1(2)\text{-}Ni}$, as well as weakening of the AFM interaction $J_{Mn1\text{-}Mn2}$ with increasing Cu content is observed, which also affects the Curie temperature of austenite (T_C^A). In the case of tetragonal structure, a weakening of FM and AFM interactions between Ni, Mn_1, Mn_2 atoms is observed. However, the Curie temperature of martensite T_C^M increases in a similar way as T_C^A. The increase in T_C^M is caused by the weakening of the strong AFM interaction between the nearest Mn_1-Mn_2, the change of which has a larger contribution to the magnetic energy compared to the change of $J_{Mn1(2)\text{-}Mn1(2)}$ and $J_{Mn1(2)\text{-}Ni}$ interactions as a function of Cu content.

Table 2. The nearest exchange coupling constants and Curie temperatures calculated within the MC method and MFA for cubic and tetragonal structures of Heusler $Ni_{50-x}Cu_xMn_{35.94}Sn_{14.06}$ alloys.

x	Mn_1-Ni	Mn_2-Ni	Mn_1-Mn_1	Mn_2-Mn_2	Mn_1-Mn_2	T_C (MC)	T_C (MFA)
FiM cubic structure							
0	2.961	2.341	1.082	-0.936	-6.065	425	423.4
1.56	2.977	2.364	1.201	-0.837	-5.925	430	433.5
3.12	2.988	2.384	1.492	-0.772	-5.859	452	444.8
4.69	2.999	2.402	1.702	-0.678	-5.722	464	453.1

Preprints (www.preprints.org) | NOT PEER-REVIEWED | Posted: 13 October 2023 doi:10.20944/preprints202310.0715.v1

FiM tetragonal structure							
0	3.514	2.308	2.035	1.859	-21.902	484	544.9
1.56	3.502	2.299	1.985	1.826	-21.513	506	547.5
3.12	3.495	2.294	1.942	1.798	-21.071	514	549.6
4.69	3.489	2.287	1.906	1.779	-20.598	523	551.4

Figure 8a shows the T-x phase diagram for $Ni_{50-x}Cu_xMn_{35.94}Sn_{14.06}$, which includes the predicted T_m and T_C temperatures and experimentally measured values of T_m and T_C^A. With increasing the Cu doping level, T_m reduces nonlinearly from 133 K (x = 0 at.%) to 88 K (x = 4.69 at.%). This is mainly due to a decrease in the energy barrier $\Delta E_{L2_1-L1_0}$ and $\Delta\Theta_D^{L2_1-L1_0}$, which have a maximum at x = 0 (see Figure 5 and Table 1). The predicted value of T_m for $Ni_{45.31}Cu_{4.69}Mn_{35.94}Sn_{14.06}$ is close to the experimental one for $Ni_{44.4}Cu_{4.5}Mn_{36.2}Sn_{14.9}$. As for Curie temperature, MC simulations and mean-field approximation (MFA) show a similar trend of T_C^A with the increase in Cu content. Nevertheless, the experimental value of T_C^A for $Ni_{44.4}Cu_{4.5}Mn_{36.2}Sn_{14.9}$ is less than the theoretical one by about 100 K.

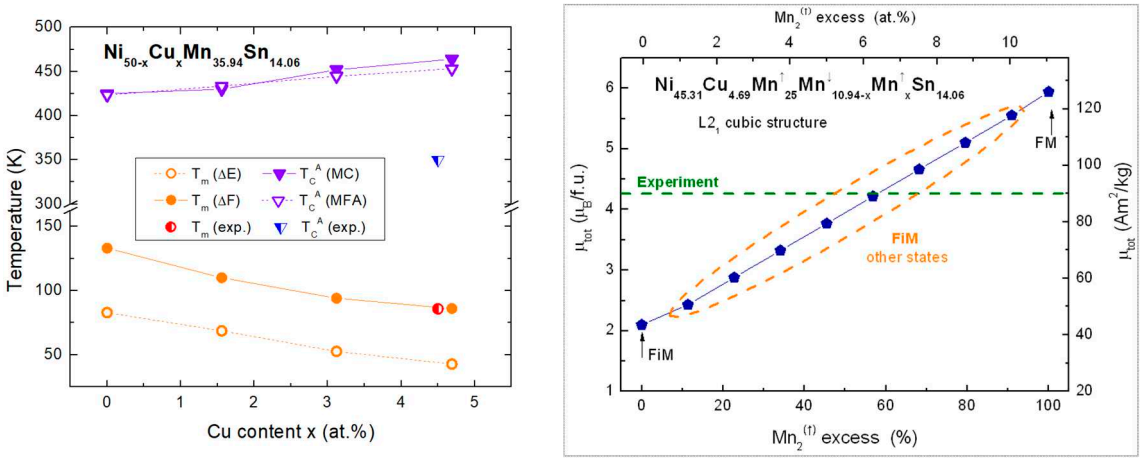

(a) **(b)**

Figure 8. (a) Calculated phase diagram for $Ni_{50-x}Cu_xMn_{35.94}Sn_{14.06}$ (x = 0, 1.56, 3.12, and 4.69). Here, T_m (ΔE) and T_m (ΔF) are the martensitic transformation temperatures calculated from energy difference at T = 0 K, which has been converted to a temperature scale, and from free energy difference considering only lattice contribution, respectively; T_C^A and T_C^M are the Curie temperatures of austenite and martensite calculated by MC method and MFA. The experimental values of T_m and T_C^A refer to $Ni_{44.4}Mn_{36.2}Sn_{14.9}Cu_{4.5}$, T_m is computed via $T_m = (M_s + M_f + A_f + A_s)/4$. (b) The calculated total magnetic moment (filled symbol) of $Ni_{45.31}Cu_{4.69}Mn_{35.94}Sn_{14.06}$ with the cubic structure as a function of Mn_2 atoms at Sn sites with a parallel magnetic moment to that of Mn_1 atoms. The experimental magnetization for austenitic phase of $Ni_{44.4}Mn_{36.2}Sn_{14.9}Cu_{4.5}$ is highlighted by the dash line.

4. Discussions

Let us next discuss the calculated total magnetic moment μ_{tot} for $Ni_{45.31}Cu_{4.69}Mn_{35.94}Sn_{14.06}$ and its relation to the experimental one for $Ni_{44.4}Cu_{4.5}Mn_{36.2}Sn_{14.9}$. It follows from Figure 6 that the magnetic reference state for both austenite and martensite is FiM one, where all magnetic moments of $Mn_1^{\uparrow}$ and $Mn_2^{\downarrow}$ are oppositely aligned. As a consequence, the μ_{tot} is calculated to be almost equal 2.16 and 2.12 μ_B or 45.6 and 44.8 emu/g, respectively. The latter value is close to the experimental magnetization of martensite (≈ 53 emu/g). However, there is some discrepancy between the calculated and measured values of μ_{tot} for austenite. The experiment yields twice larger μ_{tot}. On the other hand, the calculated value of μ_{tot} for FM austenite, which is energetically unfavorable, is about 5.94μ_B or 125.6 emu/g is larger than experimental one. The dashed line in Figure 2a are calculated curve (approximation) of the temperature dependence of the magnetization in $\mu_0 H$ = 3T for the sample in austenite phase without a magnetostructural PT. This curve was calculated by using

Preprints (www.preprints.org) | NOT PEER-REVIEWED | Posted: 13 October 2023 doi:10.20944/preprints202310.0715.v1

the approach proposed in [35]. The obtained magnetization value is 110 emu/g by using this approach (Figure 2a).

To explain the observed discrepancy, we suggest that not all Mn_2 atoms located at the Sn sublattice have antiparallel magnetic moment with respect to Mn_1 atoms located at the regular Mn sublattice. To prove this, we additionally preformed CPA calculations of μ_{tot} for L2$_1$-$Ni_{45.31}Cu_{4.69}Mn_{35.94}Sn_{14.06}$ (or $Ni_{45.31}Cu_{4.69}Mn^{\uparrow}_{25}Mn^{\downarrow}_{10.94-x}Mn^{\uparrow}_{x}Sn_{14.06}$) using SPR-KKR code as function of Mn_2 atoms at Sn sites with a parallel magnetic moment to that of Mn_1 atoms, as shown in Figure 8b. As can be seen from the figure, μ_{tot} increases linearly with a fraction of $Mn^{\uparrow}_2$ atoms and reaches 5.94 μ_B or 125.6 emu/g for 100 % amount of $Mn^{\uparrow}_2$ spins aligned parallel to $Mn^{\uparrow}_1$ ones (FM order). We find that the experimental value of μ_{tot} can be reached theoretically if only ≈40 % of Mn_2 atoms interact antiferromagnetically with Mn_1 atoms. This finding allows to conclude that the experimental sample has some kind of FiM order with the predominant amount of FM ordered Mn atoms.

The inverse MCE at low temperatures in the Heusler $Ni_{33.7}Co_{14.8}Mn_{35.4}Ti_{16.1}$ alloy show the similar values at low temperatures [19]: maximal ΔT_{ad} = –2.7 K at T_0 = 90 K in magnetic field of 20 T. Perhaps this is a physical limit on the value of the inverse MCE for the Heusler alloys with PTs at low temperatures, which is significantly lower than in known alloys with inverse MCE at room temperatures [36].

5. Conclusions

The inverse MCE in the Heusler $Ni_{33.7}Co_{14.8}Mn_{35.4}Ti_{16.1}$ alloy in the region of low temperatures is observed in magnetic field of 1.8 T in both regimes of measuring: at sequential heating and at thermal cycling. The maximum value of the inverse MCE in the vicinity of the 1st order PT in magnetic field of 1.8 T was observed
ΔT_{ad} = –0.5 K at an initial temperature T_0 = 117 K. The inverse MCE is reaching up to ΔT_{ad} = –2.7 K at T_0 = 117 K with increasing of the magnetic field up to 10 T. The direct MCE in the FiM martensite phase is observed in magnetic field of 10 T and reaching the mximal value ΔT_{ad} = 0.7 K at the sequential heating regime in the temperature range of 20–60 K.

First principles and MC approaches applied to determine the phase diagram for $Ni_{50-x}Cu_xMn_{35.94}Sn_{14.06}$ (x = 0, 1.56, 3.12, and 4.69) compounds FM ordered, which are similar in composition with experimental sample. It is shown that the Cu doping leads to decrease in T_m temperature and an increase in $T_C{}^A$ temperature. This is mainly due to the slight change in the optimized lattice constants, magnetic exchange interactions and Debye temperatures for austenite and martensite. From the analysis of our computational results, we suggest that the experimental sample exhibits some type of FiM order in the austenite, with a predominance of ferromagnetically ordered Mn atoms. The theory is well confirmed by experiment and will make it possible to predict the transition temperatures, the magnetizations and the MCE properties of Heusler Ni-Mn-Sn family when the part of Sn atoms replaced by Cu.

Author Contributions: Conceptualization, A.P.K., V.G.S.; Methodology, Y.S.K. and V.D.B.; Software, V.V.S.; Formal analysis, A.P.K., Y.S.K. and V.V.S.; Investigation, Y.S.K., A.V.K., A.V.M., R.Y.G, I.I.M., J.C. and V.V.S.; Writing—original draft, A.P.K., Y.S.K., and V.V.S.; Supervision, V.D.B. and V.G.S.; Project administration, V.G.S. All authors of the manuscript contributed equally to data acquisition and analysis, writing, editing and formatting. All authors have read and agreed to the published version of the manuscript.

Funding: The magnetization and MCE measurements were carried out within the framework of RSF project № 20-19-00745-П, https://rscf.ru/project/23-19-45040/. The alloy preparing and the structure analysis were carried out by R.Y.G and I.I.M. within the framework of the state task of IMSP RAS. V.V.S. acknowledges the financial support from the Priority-2030 Program of NUST "MISiS" (grant No. K2-2022-022) (the total energy calculations). V.D.B. acknowledge the Ministry of Science and Higher Education of the Russian Federation within the Russian State Assignment, under Contract 075-01493-23-00 (the phonon calculations).

Data Availability Statement: The data presented in this study are available on request from the corresponding author.

Acknowledgments: In this section, you can acknowledge any support given which is not covered by the author contribution or funding sections. This may include administrative and technical support, or donations in kind (e.g., materials used for experiments).

Conflicts of Interest: The authors declare no conflict of interest.

References

1. Giauque, W. F.; MacDougall, D. P. Attainment of Temperatures Below 1 Absolute by Demagnetization of $Gd_2(SO_4)_3 \cdot 8H_2O$. *Phys. Rev.* **1933**, *43*, 768.
2. Koshkid'ko, Yu. S.; Dilmieva, E. T.; Kamantsev, A. P.; Mashirov, A. V.; Cwik, J.; Kol'chugina, N. B.; Koledov, V. V.; Shavrov, V. G. Magnetocaloric Materials for Low-Temperature Magnetic Cooling. *J. Commun. Technol. Electr.* **2023**, *68*, 379–388.
3. Tishin, A. M.; Spichkin, Y. I. *The Magnetocaloric Effect and its Applications*. Publisher: IOP Publ., Bristol, 2003; 476 p. .
4. Belov, K. P. *The Magnetothermal Phenomena in Rare-Earth Magnetics.* Publisher: Nauka, Moscow, 1990.
5. Khovaylo, V. V.; Taskaev, S. V. Magnetic Refrigeration: From Theory to Applications. *Encycl. Smart Mater.* **2022**, *5*, 407–417.
6. Zhang, H.; Sun, Y. J.; Niu, E.; Yang, L. H.; Shen, J.; Hu, F. X.; Sun, J. R.; Shen, B. G. Large magnetocaloric effects of RFeSi (R = Tb and Dy) compounds for magnetic refrigeration in nitrogen and natural gas liquefaction. *Appl. Phys. Lett.* **2013**, *103*, 202412.
7. Timmerhaus, K. D.; Reed, R. P. *Cryogenic Engineering: Fifty Years of Progress.* Publisher: Springer Science & Business Media, New York, 2007.
8. Suslov, D. A.; Shavrov, V. G.; Koledov, V. V.; Mashirov, A. V.; Terentyev, Yu. A.; Petrov, A. O.; Kamantsev, A. P.; Samvelov, A. V.; Yasev, S. G.; Taskaev, S. V.; Kolesov, K. A. Comparison of thermodynamic efficiency of cryogenic gas and solid-state magnetocaloric cycles. *Chel. Phys.-Math. J.* **2020**, *5*, 612–617.
9. Andreenko, A. S.; Belov, K. P.; Nikitin, S. A.; Tishin, A. M. Magnetocaloric effects in rare-earth magnetic materials. *Sov. Phys. Usp.* **1989**, *32*, 649–664.
10. Zheng, X. Q.; Xu, Z. Y.; Zhang, B.; Hu, F. X.; Shen, B. G. The normal and inverse magnetocaloric effect in RCu_2 (R= Tb, Dy, Ho, Er) compounds. *J. Magn. Magn. Mater.* **2017**, *421*, 448–452.
11. Kamantsev, A. P.; Koshkidko, Y. S.; Taskaev, S. V.; Khovaylo, V. V.; Koshelev, A. V.; Cwik, J.; Shavrov, V. G. Inverse Magnetocaloric Effect and Kinetic Arrest Behavior in As-Cast Gd_2In at Cryogenic Temperatures. *J. Supercond. Nov. Magn.* **2022**, *35*, 2181–2186.
12. Nikitin, S. A.; Skokov, K. P.; Koshkid'ko, Yu. S.; Pastushenkov, Yu. G.; Ivanova, T. I. Giant Rotating Magnetocaloric Effect in the Region of Spin-Reorientation Transition in the $NdCo_5$ Single Crystal. *Phys. Rev. Lett.* **2010**, *105*, 137205.
13. Nikitin, S. A.; Ivanova, T. I.; Zvonov, A. I.; Koshkid'ko, Yu.S.; Ćwik, J.; Rogacki, K. Magnetization, magnetic anisotropy and magnetocaloric effect of the $Tb_{0.2}Gd_{0.8}$ single crystal in high magnetic fields up to 14 T in region of a phase transition. *Acta Mater.* **2018**, *161*, 331.
14. Kuznetsov, A. S.; Mashirov, A. V.; Musabirov, I. I.; Mitsiuk, V. I.; Anikin, M. S.; Kamantsev, A. P.; Koledov, V. V.; Shavrov, V. G. Inverse Magnetocaloric Effect in Mn_5Si_3 Compound. *J. Commun. Technol. Electr.* **2023**, *68*, 413–419.
15. Koshkid'ko, Y.; Cwik, J.; Dilmieva, E.; Pandey, S.; Quetz, A.; Aryal, A.; Dubenko, I.; Ali, N.; Granovsky, A.; Lähderanta, E.; Zhukov, A.; Stadler, S. Inverse magnetocaloric effects in metamagnetic Ni-Mn-In-based alloys in high magnetic fields. *J. Alloy. Compd.* **2017**, *695*, 3348–3352.
16. Dilmieva, E. T.; Koshkid'ko, Yu. S.; Kamantsev, A. P.; Koledov, V. V.; Mashirov, A. V.; Shavrov, V. G.; Khovaylo, V. V.; Lyange, M. V.; Cwik, J.; Gonzalez-Legarreta, L.; Grande, H. B. Research of magnetocaloric effect of Ni-Mn-In-Co Heusler alloys by the direct method in magnetic fields up to 14 T. *IEEE Trans. Magn.* **2017**, *53*, 2503705.
17. Konoplyuk, S. M.; Kokorin, V. V.; Mashirov, A. V.; Kamantsev, A. P.; Koledov, V. V.; Shavrov, V. G.; Koshelev, A.V. Direct measurements of adiabatic temperature change in $Ni_{49.9}Mn_{37.03}Sb_{12.3}Fe_{0.77}$ alloy due to magnetocaloric effect in the temperature range of martensitic transformation. *IEEE Trans. Magn.* **2018**, *54*, 2500204.
18. Sokolovskii, V. V.; Nachinova, D. V.; Buchel'nikov, V. D.; Dilmieva, E. T.; Koshkidko, Yu. S.; Emelyanova S. M.; Marchenkova, E. B.; Marchenkov, V. V. Magnetic and magnetocaloric properies of Heusler alloys Ni-Mn-Sn with an excess of Mn within the theoreticaland experimental approaches. *Chel. Phys.-Math. J.* **2020**, *5*, 493–503.

19. Beckmann, B.; Koch, D.; Pfeuffer, L.; Gottschall, T.; Taubel, A.; Adabifiroozjaei, E.; Miroshkina, O. N.; Riegg, S.; Niehoff, T.; Kani, N. A.; Gruner, M. E.; Molina-Luna, L.; Skokov, K. P.; Gutfleisch, O. Dissipation losses limiting first-order phase transition materials in cryogenic caloric cooling: A case study on all-d-metal Ni (-Co)-Mn-Ti Heusler alloys. *Acta Mater.* **2023**, *246*, 118695.
20. Elerman, Y.; Dinçer, I.; Yüzüak, E.; Emre, B.; Yüce, S.; Ener, S.; Akarca, B. *Ferromanyetik Ni-ve Co-tabanlı Heusler alaşımlarının yapısal, manyetokalorik, ısısal, elektriksel ve spintronik özelliklerinin incelenmesi*. Publisher: Ankara Üniversitesi Bilimsel Araştırma Projeleri, 2011, 48 p. http://hdl.handle.net/20.500.12575/69958
21. Gaifullin, R.Yu.; Kirilyuk, K.K.; Safarov, I.M.; Musabirov, I.I. Structure of $Ni_{44.4}Mn_{36.2}Sn_{14.9}Cu_{4.5}$ alloy applicable for thermomechanical treatment. *Lett. Mater.*, **2023**, *13(2)*, 164-170.
22. Anand, A.; Manjuladevi, M.; Veena, R. K.; Veena, V. S.; Koshkid'ko, Y. S.; Sagar, S. A study on spin memory, nature of magnetic transition, and magnetocaloric effect in $Nd_{0.5}Ca_{0.5}MnO_3$. *J. Magn. Magn. Mater.* **2021**, *528*, 167810.
23. Kresse, G.; Furthmüller, J. Efficient iterative schemes for ab initio total-energy calculations using a plane-wave basis set. *Phys. Rev. B.* **1996**, *54*, 11169-11186.
24. Kresse, G.; Joubert, D. From ultrasoft pseudopo-tentials to the projector augmented-wave method. *Phys. Rev. B* **1999**, *59*, 1758-1775.
25. Perdew, J. P.; Burke, K.; Ernzerhof, M. Generalized Gradient Approximation Made Simple. *Phys. Rev. Lett.* **1996**, *77*, 3865-3868.
26. Ebert, H.; Ködderitzsch, D.; Minár, J. Calculating condensed matter properties using the KKR-Green's function method-recent developments and applications. *Rep. Prog. Phys.* **2011**, *74*, 096501-48.
27. Landau, D.; Binder K. *A guide to Monte Carlo simulations in statistical physics*; Publisher: Cambridge university press, 2021, p. 578.
28. Koshkid'ko, Y. S.; Dilmieva, E. T.; Cwik, J.; Rogacki, K.; Kowalska, D.; Kamantsev, A. P.; Koledov, V.V.; Mashirov, A.V.; Shavrov, V.G.; Valkov, V.I.; Golovchan, A.V.; Sivachenko, A.P.; Shevyrtalov, S.N.; Rodionova, V.V.; Shchetinin, I.V.; Sampath, V. Giant reversible adiabatic temperature change and isothermal heat transfer of MnAs single crystals studied by direct method in high magnetic fields. *J. Alloyю Comp.* **2019**, *798*, 810-819.
29. Koshkid'ko, Y. S.; Ćwik, J.; Ivanova, T. I.; Nikitin, S. A.; Miller, M.; Rogacki, K. Magnetocaloric properties of Gd in fields up to 14 T. *J. Magn. Magn. Mater.* **2017**, *433*, 234-238.
30. Moruzzi, V. L.; Janak, J. F.; Schwarz, K. Calculated thermal properties of metals. *Phys. Rev. B* **1988**, *37*, 790 – 799.
31. Comtesse, D.; Gruner, M.E.; Ogura, M.; Sokolovskiy, V.V.; Buchelnikov, V.D.; Gru¨nebohm, A.; Arróyave, R.; Singh, N.; Gottschall, T.; Gutfleisch, O.; et al. First-principles calculation of the instability leading to giant inverse magnetocaloric effects. *Phys. Rev. B* **2014**, *89*, 184403-6.
32. Sokolovskiy, V.V.; Buchelnikov, V.D.; Zagrebin, M.A.; Entel, P.; Sahool, S.; Ogura, M. First-principles investigation of chemical and structural disorder in magnetic $Ni_2Mn_{1+x}Sn_{1-x}$ Heusler alloys. *Phys. Rev. B.* **2012**, *86*, 134418-11.
33. Sokolovskiy, V.; Gru¨nebohm, A.; Buchelnikov, V.; Entel, P. Ab initio and Monte Carlo approaches for the magnetocaloric effect in Co- and In-doped Ni-Mn-Ga Heusler alloys. *Entropy.* **2014**, *16*, 4992-5019.
34. Buchelnikov, V.D.; Sokolovskiy, V.V.; Zagrebin, M.A.; Klyuchnikova, M.A.; Entel, P. First-principles study of the structural and magnetic properties of the $Ni_{45}Co_5Mn_{39}Sn_{11}$ Heusler alloy. *J. Magn. Magn. Mater.* **2015**, *383*, 180-185.
35. Kuz'min, M. D. Landau-type parametrization of the equation of state of a ferromagnet. *Phys. Rev. B*, **2008**, *77*, 184431.
36. Kamantsev, A.P.; Amirov, A.A.; Zaporozhets, V.D.; Gribanov, I.F.; Golovchan, A.V.; Valkov, V.I.; Pavlukhina, O.O.; Sokolovskiy, V.V.; Buchelnikov, V.D.; Aliev, A.M.; Koledov V.V. Effect of Magnetic Field and Hydrostatic Pressure on Metamagnetic Isostructural Phase Transition and Multicaloric Response of $Fe_{49}Rh_{51}$ Alloy. *Metals.* **2023,** *13*, 956.